RSC Advances

PAPER

View Article Online
View Journal | View Issue

Cite this: *RSC Adv.*, 2018, **8**, 35294

Synthesis of ordered Ca- and Li-doped mesoporous silicas for H_2 and CO_2 adsorption at ambient temperature and pressure†

Nabanita Pal, *[a] Taeyeon Kim,[b] Jae-Seo Park[b] and Eun-Bum Cho *[b]

Ca- and Li-doped mesoporous silicas have been prepared successfully using cetyltrimethylammonium bromide (CTAB) surfactant in basic media. Sol–gel synthesis and hydrothermal treatment produced highly ordered mesoporous Ca and Li loaded silica particles. The MCM-41 type mesostructures, the porosity, the pore sizes as well as the surface area of Ca- and Li-silicas have been thoroughly investigated using small angle X-ray scattering (SAXS), transmission electron microscopy (TEM), and N_2 sorption analysis. Samples prepared with varying amounts of Li and Ca loading have been further analyzed using inductive coupled plasma-atomic emission spectroscopy (ICP-AES) and field-emission scanning electron microscopy (FESEM) with an energy dispersive spectral attachment (EDS), which confirmed quite a large amount of Ca while the amount of Li was not enough. Additionally, H_2 and CO_2 gas uptake studies of these metal-loaded silicas have been carried out using a thermogravimetric analyzer (TGA) at normal temperature (25 °C) and pressure (1 atm). H_2 uptake of up to 10 mmol g^{-1} by Ca-doped silica was recorded. CO_2 and H_2 selectivity were tested with both pure metal-MCM-41 and amine loaded silica using pure N_2 gas and a mixed flow of CO_2/N_2 and H_2/N_2. The effect of temperature on CO_2 uptake was also studied using Ca-MCM-41 materials.

Received 6th July 2018
Accepted 3rd October 2018

DOI: 10.1039/c8ra05772a

rsc.li/rsc-advances

1. Introduction

With the indiscriminate use of fossil fuels that began in the 18th century, the world is heading towards the culmination of global warming. About 300 years ago, the average carbon dioxide (CO_2) concentration of the Earth was about 280 ppm. However, since 1750, when the first industrial revolution began, the average concentration of CO_2 has risen sharply, now approaching 380 ppm.[1] A dramatic increase in CO_2 concentration is the main cause of the greenhouse effect as well as global warming, which is one of the biggest concerns for the modern world.[2] Although an enormous study on the development of various renewable alternatives to conventional carbon-based energy sources is going on, it is still very unrealistic to imagine a future world without burning carbon based fossil fuels. Since thermal power plants are the main source of CO_2 emission in the environment, it will be more effective to capture and remove CO_2 from power plant fuel gas using a cost-effective material which will reduce the atmospheric CO_2 concentration to a large extent. A number of CO_2 adsorbing materials have been reported as potential candidates for use as CO_2 adsorbents for industrial purposes.[2]

Another way to solve the problems related to global warming and a large quantity of CO_2 emission is to find any alternative energy sources that can replace the fossil fuels used for centuries. Hydrogen energy is known as a 'green' alternative and renewable energy source for vehicles that could be available now.[3,4] However, as is already well known, hydrogen is the lightest gas and has high flammability, which make it extremely difficult to store H_2. Therefore, an ideal hydrogen storage material should meet the various requirements of industry: for example, high capacity, fast dynamics, and fast adsorption and desorption which will make hydrogen easy to handle.[5]

Conventional hydrogen storage devices use either pressurized tanks of pure gas or liquid hydrogen at cryogenic temperatures.[6] However, the simplest method used nowadays is to physically adsorb and store hydrogen on the surface of a suitable material.[6] Several researchers have attempted to store hydrogen effectively using nanoporous materials with high gravimetric and volumetric densities.[7,8] Materials with high specific surface areas, such as microporous zeolites,[9,10] mesoporous silica, carbon[11] and metal–organic frameworks (MOFs),[12] are worthy of mention in this case. Some other significant adsorbents like nitrilotriacetic acid anhydride (NTAA) modified ligno-cellulosic material,[13] dried biomass[14] or biofilm[15] waste from biotrickling filters are environmentally

[a]Faculty of Science and Technology, The ICFAI Foundation for Higher Education, Donthanapally, Shankarapalli Road, Hyderabad-501203, India. E-mail: naba.p27@gmail.com

[b]Department of Fine Chemistry, Seoul National University of Science and Technology, 232 Gongneung-ro, Nowon-gu, Seoul 01811, Republic of Korea. E-mail: echo@seoultech.ac.kr

† Electronic supplementary information (ESI) available. See DOI: 10.1039/c8ra05772a

friendly and highly biodegradable, but effective for the removal only of heavy metal ions like Cd(II) or Pd(II) from aqueous solution. So, from an economic point of view, it will be highly cost-effective to fabricate suitable nanoporous materials which will be ideal for both H_2 and CO_2 gas storage. Very recently, Cho *et al.* reported the synthesis of thermally stable hydrogen titanate ($H_2Ti_3O_7$) nanotubes with nanopores to analyze their adsorption performance for H_2 and CO_2 gases.[16]

In the last few decades, silica-based porous solids have been proved to be effective materials for H_2 and CO_2 gas adsorption.[17] MCM-41, a typical porous material, synthesized for refining petroleum at Mobil Oil Corporation, exhibits high surface area, large pore size, and high pore volume.[18] In addition, in the case of surface modification with amines, CO_2 can be captured by reversibly reacting with amine groups to form carbamate, carbonate and bicarbonate species and thus the adsorption capacity on MCM-41 can be increased further.[2,19] For example, MCM-41 loaded with 75 wt% polyethylenimine (PEI) showed a significant increase in CO_2 adsorption in pure CO_2 atmosphere.[1]

Generally, alkali- and alkaline earth metal oxides exhibit a basic property. Therefore, the process of capturing Lewis acidic CO_2 with metallic oxides is a technique widely used in industry.[20] In particular, the process of capturing CO_2 using CaO is known as "carbonate looping". This process is a solid–gas reversible and exothermic reaction between CaO and CO_2 to produce $CaCO_3$.[21] When heat is applied, the reaction is reversed and both CaO and CO_2 are produced again. Furthermore, Jian hui Lan *et al.* reported that alkali metal oxides are also effective in adsorption of H_2.[5] They synthesized Li-doped silica fullerenes by using the fact that the basic alkali metal oxide gives a polarity to the hydrogen gas through the charge transfer mechanism, resulting in a strong bond between the metal oxide and H_2.[5] In this way, it can be said that the capture of CO_2 and H_2 using a metal oxide is a reasonable method.

Thus, a combination of high surface area MCM-41 materials with basic metal ions will have high potential and be cost-effective for CO_2 and H_2 storage compared to other bio-adsorbents. Additionally these composite materials are very easy to synthesize using a cationic surfactant, metal and tetraethyl orthosilicate (TEOS) as a silica precursor *via* a sol–gel condensation reaction in basic conditions, owing to the electrostatic interaction of cationic surfactant and hydrolysed anionic silica precursor.[22] In particular, there are very few previous reports in the literature showing the characteristics of both CO_2 capture and H_2 storage ability at ambient temperature and pressure.[23]

Herein, we report new mesoporous MCM-41 type materials doped with various percentages of Li ions (Li-MCM-41) and Ca ions (Ca-MCM-41) synthesized in a simple sol–gel route using a CTAB template, metal, silica precursors, NH_3 base and water-ethanol solvent mixture. The physical and chemical structures of the Li-MCM-41 and Ca-MCM-41 samples have been thoroughly characterized; the adsorption performance of H_2 and CO_2 gases has been investigated at ambient pressure and temperature and the reversibility for gas uptake was also tested.

2. Experimental details

2.1. Materials

Hexadecyltrimethylammoniumbromide (CTAB, 98%) and tetraethylorthosilicate (TEOS, 98%) were used as a structure-directing agent and silica precursor, respectively. Ammonium hydroxide (NH_4OH, 28.0–30.0% NH_3) solution and ethanol (EtOH) were used as a basic catalyst and solvent, respectively. Lithium(I) nitrate ($LiNO_3$), calcium(II) nitrate tetrahydrate ($Ca(NO_3)_2 \cdot 4H_2O$) and calcium(II) hydroxide ($Ca(OH)_2$) were used as metal precursors. *N*-[3-(Trimethoxysilyl)propyl]ethylenediamine (TSPED) was used to functionalize the pore walls of Ca- and Li-doped mesoporous silica materials. Deionized water prepared in our laboratory was used as one of the solvents for the preparation of all the samples studied. All chemicals were purchased from Sigma-Aldrich and used as received without further purification.

2.2. Synthetic procedure

2.2.1. Li-doped mesoporous silica. In a typical synthesis of Li-doped silica composites with Li/Si = 0.1, CTAB (1.5 g, 4.1 mmol) was dissolved completely in a mixture of 30 mL of deionized water and 45.6 mL of ethanol under vigorous stirring. This was followed by the addition of 35 mL (0.5 mol) of NH_4OH to achieve basic conditions. After continuous stirring for 30 min at room temperature, 3.0 mL (13.4 mmol) of TEOS was added to the solution. After stirring the solution at a constant speed of 500 rpm for a further 30 min, 0.092 g (1.34 mmol) of $LiNO_3$, was added to the mixture and the resulting mixture was stirred continuously for a further 24 h at room temperature. Finally, the mixture was aged for 24 h at 100 °C in a convection oven. To remove the excess of surfactant, solvents, and unreacted species, the mixture was filtered and washed with an adequate amount of deionized water and ethanol, and then dried in air. The collected as-synthesized product was heated at a rate of 3 °C min^{-1} and calcined at 550 °C for 5 h under flowing air to remove the surfactant template. The final white powder is named LHMS-1. The syntheses of the other samples with Li/Si = 0.2, 0.3 and 0.5 (LHMS-2, -3, -5) were performed using similar methods but with varying amounts of Li source.

2.2.2. Ca-doped mesoporous silica. In a typical synthesis of Ca-doped silica composites with Ca/Si = 0.1, CTAB (1.5 g, 4.1 mmol) was dissolved completely in a mixture of 30 mL of deionized water and 45.6 mL of ethanol under vigorous stirring. This was followed by the addition of 35 mL (0.5 mol) of NH_4OH to achieve basic conditions. After continuous stirring for 30 min at room temperature, 3.0 mL (13.4 mmol) of TEOS was added to the solution. After stirring the solution at a constant speed of 500 rpm for a further 30 min, 0.32 g (1.34 mmol) of $Ca(NO_3)_2$, and 0.1 g (1.34 mmol) (when using $Ca(OH)_2$) were added to the mixture and the resulting mixture was stirred continuously for a further 24 h at room temperature. Finally, the mixture was aged for 24 h at 550 °C in a convection oven. To remove the excess of surfactant, solvents, and unreacted species, the mixture was filtered and washed with an adequate amount of deionized water and ethanol, and then dried in air. The

collected as-synthesized product was heated at a rate of 3 °C min^{-1} and calcined at 550 °C for 5 h under flowing air to remove the surfactant template. The final white solid obtained after calcination was named CHMS-1. Following similar methods the syntheses of other samples with Ca/Si = 0.2, 0.3 and 0.5 (CHMS-2, -3, -5) were carried out with varying amounts of both Ca sources (calcium nitrate and calcium hydroxide).

2.2.3. Amine functionalization. In a typical preparation, 1 g of mesoporous material and 0.6 mL of amine-containing TSPED organosilane precursor were mixed in a 125 mL glass bottle containing 50 mL of toluene. The mixture was stirred magnetically in an oil bath at 90 °C for 20 h. The final solid product was obtained after filtration with an adequate amount of ethanol and acetone.

2.3. Characterizations

The lithium and calcium weight percentages in the respective samples were determined by Jobin Yvon inductively coupled plasma (ICP) (ICP-OES, JY Ultima 2C) analysis at the KBSI Seoul Center. Data were obtained by calculating the average value from three sets of measurements.

Small-angle X-ray scattering (SAXS) experiments for all the LHMS and CHMS samples were performed using Synchrotron radiation with $\lambda = 1.608$ Å, at the 3C and 4C lines of the Pohang Accelerator Laboratory in POSTECH. The distance between the sample and detector was set at 1 m for each experiment, and the sample exposure time was 0.1 to 1 s for each sample. The data were obtained in the rage $q = 0.05$–0.55 $Å^{-1}$ by converting the signals collected by a 2D detector using 2D data processing software.

Wide angle X-ray diffraction (XRD) analysis was performed using a PANalytical Empyrean multipurpose diffractometer with Cu-K_α radiation ($\lambda_{avg} = 0.15418$ nm) at 40 kV and 30 mA in the Korea Basic Science Institute (KBSI) Daegu Center. The spectra were collected at $2\theta = 10$ to 90° with a scan rate of 0.04° s^{-1}.

Macroscopic morphological images were obtained using a field emission scanning electron microscope (FE-SEM) (JEOL JSM-4300F) equipped with an embedded EDS system and operated at an accelerating voltage of 15 kV. The mesopore structures of the samples were obtained using a FEI TECNAI G^2 F30 ST transmission electron microscope (TEM) operated at an accelerating voltage of 200 kV. Prior to the analysis, the samples were prepared by proper sonication for 30 min dispersing in acetone and the solutions were then dropped onto a porous carbon film on a copper grid and then dried in air.

Nitrogen adsorption isotherms were measured using a Micromeritics 2420 analyzer at −196 °C. Before the analysis, all the samples were degassed at 500 °C under vacuum below 30 μmHg for at least 3 h. The Brunauer–Emmett–Teller (BET) specific surface area was calculated from the adsorption isotherm at relative pressures (P/P_0) from 0.04 to 0.2. The total pore volume was evaluated from the amount adsorbed at a relative pressure of 0.99. The pore size distribution (PSD) curves were calculated from the adsorption isotherms by using the improved Kruk–Jaroniec–Sayari (KJS) method.[24] The pore wall thickness (W) was estimated from the pore size (D_{KJS}) obtained at the maximum of PSD and the unit cell parameter (a) obtained by SAXS.

2.4. H_2 and CO_2 adsorption

Both the adsorption measurements of H_2 and CO_2 gases were performed using a microbalance inside a Q50 thermogravimetric analyzer (TA instrument). Prior to measuring the gas uptake, all samples were kept in a vacuum oven for 24 h. Approximately 10 mg of the Ca- and Li-doped silica samples were loaded on the sample plate and sealed in the cylindrical chamber. In the initial stage, the cylindrical chamber was purged with flowing N_2 gas at 100 mL min^{-1} at 110 °C for 2 h. Then, the chamber was cooled down to 25 °C under continuous N_2 flow and the gas uptake was recorded for 3 h in a flowing mixture of N_2 gas at 40 mL min^{-1} and CO_2 gas at 60 mL min^{-1}. The same procedure was applied to analyze H_2 gas uptake for pure CHMS and LHMS samples using a mixture of flowing N_2 gas at 40 mL min^{-1} and H_2 gas at 60 mL min^{-1} at 25 °C. Adsorption measurements at a higher temperature of 120 °C at a heating rate of 1 °C min^{-1} were also conducted to study the effects of temperature on the CO_2 adsorption capacities of Ca-doped silica materials.

3. Results and discussions

3.1. Synchrotron small angle X-ray scattering (SAXS) analysis

Synchrotron SAXS analysis was carried out to get information about the mesostructures of the calcined metal doped mesoporous silica materials. SAXS data of all Ca- and Li-doped silica samples are given in Fig. 1(a) and (b), respectively. Well-defined peaks with several intensities are observed from Ca-doped CHMS samples with Ca/Si ratios 0.1, 0.2, 0.3 and 0.5 (Fig. 1(a)). CHMS-1, CHMS-2 and CHMS-5 show a major peak indexed as the (100) plane, with other small intense peaks assigned to (110) and (200) planes, according to the *p6mm* symmetry group, which indicate that a highly ordered 2D hexagonal mesostructure has been formed with the CHMS samples.[25] It is also clear from Fig. 1(a) that, with increasing Ca content the peak intensity decreases, indicating a decrease in ordered porosity. This type of phenomenon is not very rare in the literature.[17] Although mesostructure formation is confirmed by the (100) peak from sample CHMS-3 with Ca/Si = 0.3, the ordered nature of the mesopores is not observed at all due to the absence of other peaks. The values of the d-spacing corresponding to the (100) plane and the calculated unit cell parameter a ($a = 2d_{100}/\sqrt{3}$ for the *p6mm* mesostructure) are listed in Table 1.

Fig. 1(b) shows similar types of well-resolved peaks for all the Li-doped silica LHMS samples. Samples with Li/Si ratios = 0.1, 0.2, 0.3 and 0.5 all indicate the formation of a highly ordered 2D hexagonal mesostructure owing to the presence of (100), (110) and (200) planes in the SAXS patterns. Similar to the CHMS samples, in the case of high content (LHMS-5), the peak intensity is a little less due to the decrease in the ordered nature of the pores. The d-spacing values and the unit cell parameters

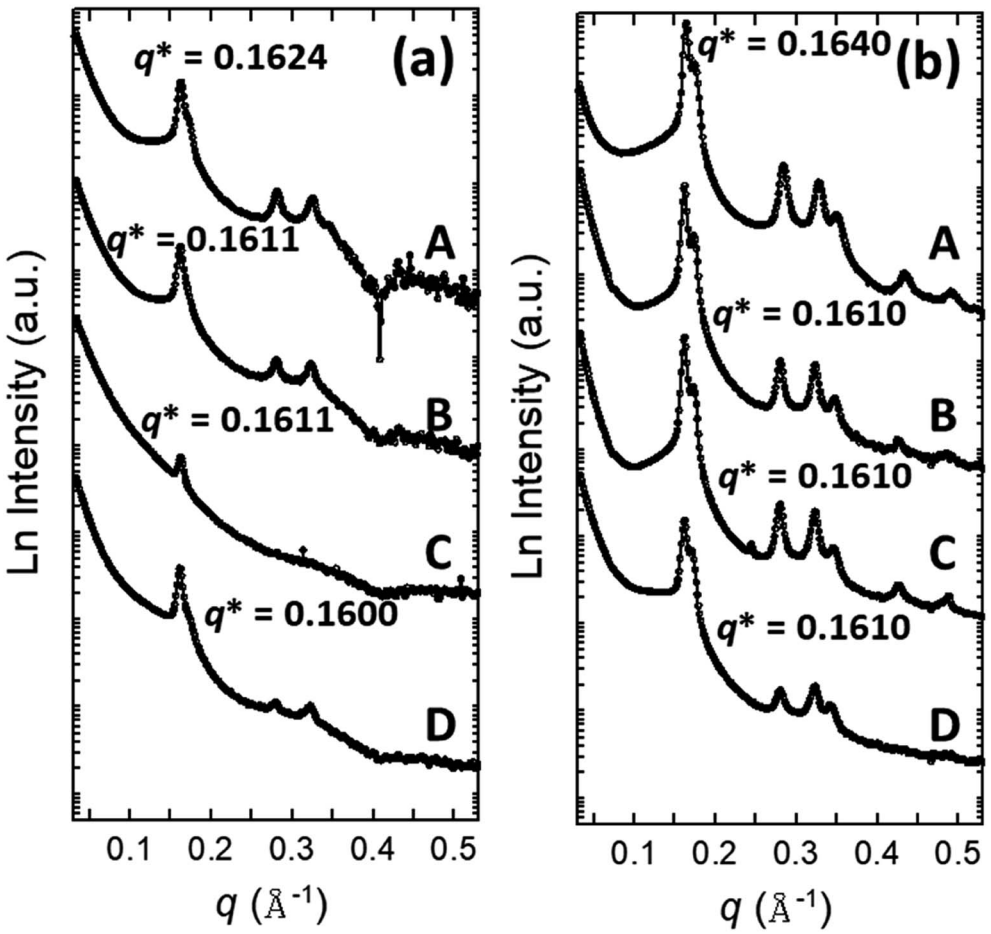

Fig. 1 Synchrotron SAXS spectra of all mesostructured MCM-41 type Ca- and Li-doped silica samples. (a) Spectra of the samples (A) CHMS-1, (B) CHMS-2, (C) CHMS-3 and (D) CHMS-5. (b) Spectra of samples named (A) LHMS-1, (B) LHMS-2, (C) LHMS-3, and (D) LHMS-5.

a, have been evaluated considering the *p6mm* mesostructure, and are given in Table 1.

3.2. Wide-angle X-ray analysis (WAXRD)

Wide-angle X-ray diffraction patterns were recorded and the data are given in ESI Fig. S1 and S2.† A broad peak for the SiO_2 phase near $2\theta = 21^\circ$ is observed, indicating the amorphous pore wall of the mesoporous silica sample.[26] There is no significant peak corresponding to any metal oxide phases of either Ca or Li. The reason is that Li and Ca ions present in these samples have been incorporated into the lattice structure of SiO_2, which is not unusual in the literature.[26] However, for samples containing a higher percentage of Ca, *viz.* CHMS-3 and CHMS-5 samples, there are small fingerprints for CaO and $Ca(OH)_2$ observed in the WAXRD data. This result implies the good incorporation of Ca ions into the lattice structure of SiO_2.

Table 1 Physicochemical data for the series of CHMS and LHMS samples[a]

Sample	S_{BET} ($m^2\ g^{-1}$)	V_P ($cm^3\ g^{-1}$)	*d*-spacing (nm)	*a* (nm)	D_{KJS} (nm)	*W* (nm)
CHMS-1	90.90	0.35	3.86	4.46	11.10	n.d.
CHMS-2	317.73	0.40	3.90	4.50	3.23	1.27
CHMS-3	35.63	0.18	3.90	4.50	15.37	n.d.
CHMS-5	315.86	0.46	3.93	4.54	3.42	1.12
LHMS-1	742.97	0.59	3.83	4.42	3.33	1.09
LHMS-2	323.51	0.39	3.90	4.50	3.23	1.27
LHMS-3	709.69	0.51	3.90	4.50	3.35	1.15
LHMS-5	543.36	0.44	3.90	4.50	3.12	1.38

[a] Notation: S_{BET} = BET specific surface area; V_P = total pore volume; *d*-spacing = Bragg spacing ($= 2\pi/q^*$), where q^* is the value of *q* at the maximum in the (100) peak for the *p6mm* mesostructure; *a* = unit cell parameter ($= 2d_{100}/\sqrt{3}$ for *p6mm* structure); D_{KJS} = mesopore diameter at the maximum in the PSD curve determined by KJS method; *W* = pore wall thickness ($= a - D_{KJS}$).

Table 2 ICP-AES data for all the CHMS and LHMS samples

Sample	Li Concentration (wt%)	Sample	Ca Concentration (wt%)
LHMS-1	<10 ppm	CHMS-1	4.54
LHMS-2	<10 ppm	CHMS-2	6.10
LHMS-3	0.0034	CHMS-3	11.98
LHMS-5	0.044	CHMS-5	14.94

3.3. Elemental analysis

The ICP-AES technique has been used to evaluate the weight percentage of Ca and Li species in the respective CHMS and LHMS samples and these are shown in Table 2. From the data, it is observed that Li incorporation into the LHMS-1 and -2 samples is almost negligible, whereas the other two samples, LHMS-3 and -5, also show a very small amount of Li content up to 0.044 wt%. CHMS samples contain Ca with weight percentages varying from 4.5 to 15, although the Ca/Si ratio is a little less than that used during synthesis. This implies that some of the metal ions have been leached without binding with the silica species through filtration as well as during the sol–gel chemical reaction, especially for alkali Li ions with a strong tendency for ionization in aqueous solution.

3.4. FESEM and EDS

The morphology and particle size of the Ca and Li-doped mesoporous silica materials are best known from the FESEM image analysis. The representative FESEM images of the CHMS-1, CHMS-2, CHMS-3 and CHMS-5 samples are shown in Fig. 2(a), (b), (c) and (d), respectively. All the CHMS samples show the formation of uniform spherical particles of sizes in the range 400–500 nm distributed throughout the specimens. LHMS samples also show a similar type of spherical particles (Fig. 3(a)–(d)), with sizes varying from 400 to 500 nm in nature.

The weight% and atomic% data of the Ca, Si and O atoms are obtained from the energy-dispersive spectrometry (EDS) of the CHMS samples and the results are given in Table 3. It is clear that from the data that the Ca/Si ratios based on the weight% data are in good agreement with the Ca/Si ratios present in the synthesis gel. Fig. 4 shows a representative EDS elemental mapping for the CHMS-5 sample, indicating the presence of all the elements Si, O and Ca in the sample. The mapping images clearly imply that all the elements are uniformly distributed throughout the specimen.

3.5. Transmission electron microscopic (TEM) analysis

Transmission electron microscopic images of the CHMS and LHMS samples have been recorded to investigate the nanostructural features at atomic level. TEM images of CHMS are given in Fig. 5(a) and (b). From the TEM image, spherical shaped particles with a size of around 500 nm have been confirmed, which was also evident from the FESEM images. The TEM image of the CHMS-5 sample observed along the (110) planes is shown in Fig. 5(b). A channel-like arrangement of (110) planes is

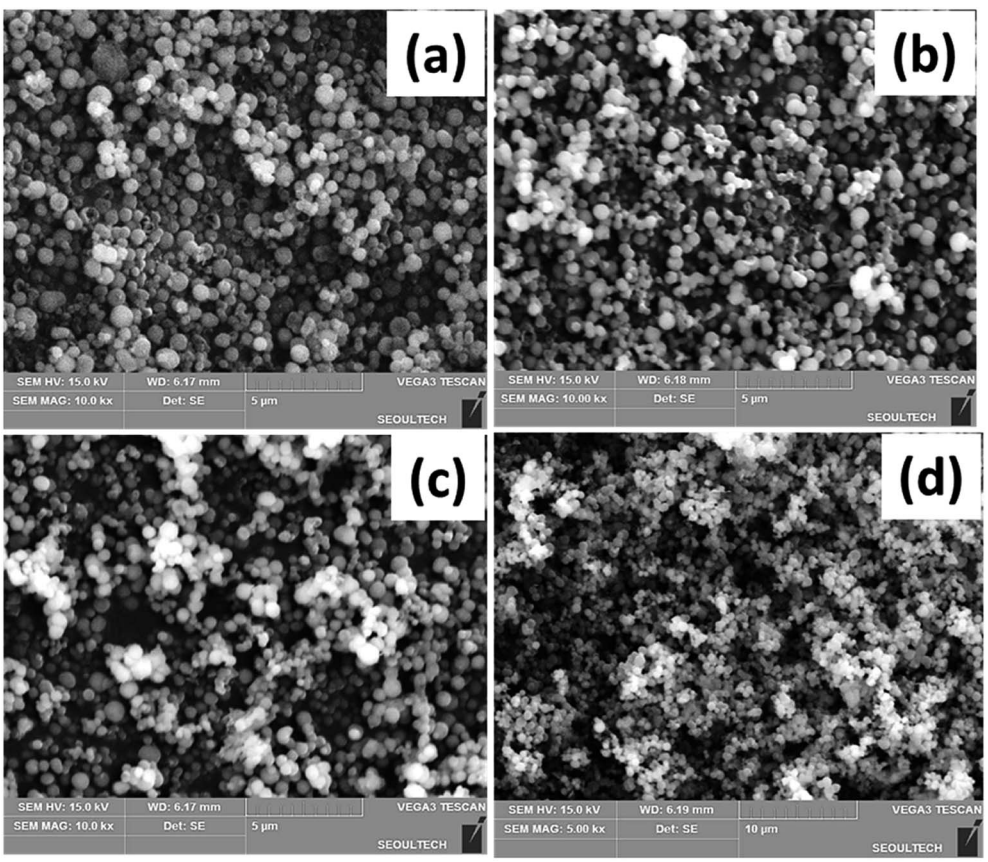

Fig. 2 FESEM images of the Ca doped hexagonal mesoporous silica samples: (a) CHMS-1, (b) CHMS-2, (c) CHMS-3, and (d) CHMS-5 samples.

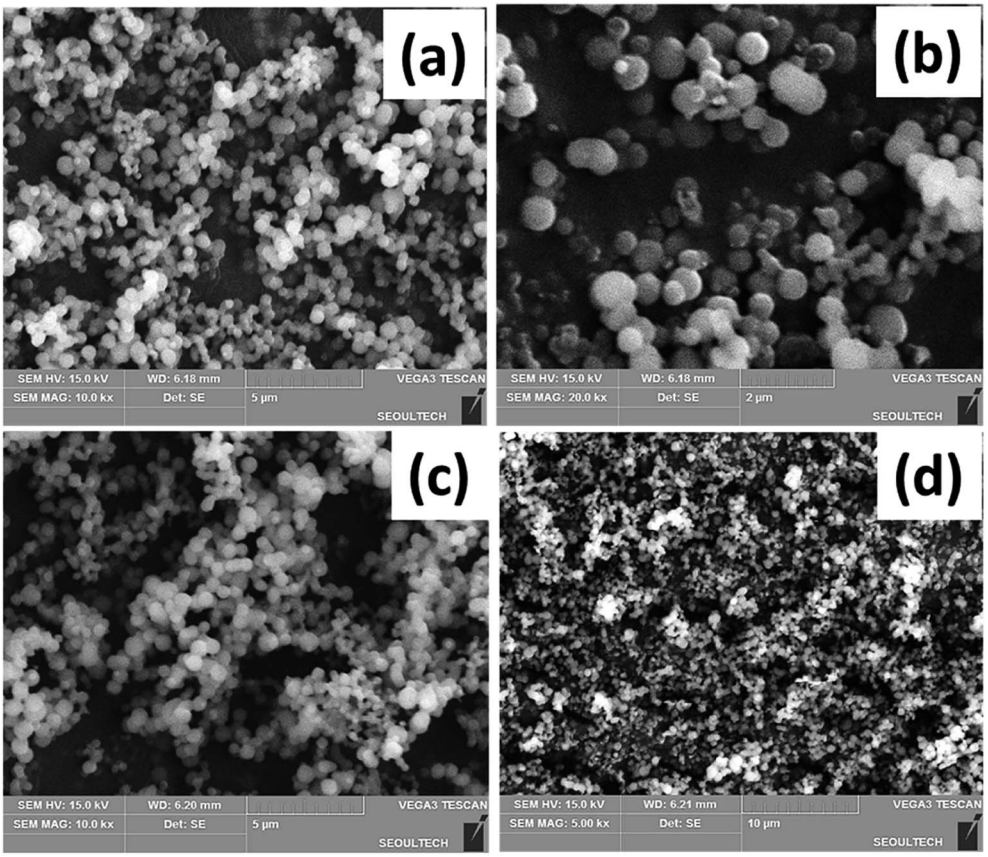

Fig. 3 FESEM images of the Li doped hexagonal mesoporous silica samples: (a) LHMS-1, (b) LHMS-2, (c) LHMS-3, and (d) LHMS-5 samples.

Table 3 SEM-EDS data for Ca doped mesoporous CHMS silica samples[a]

Sample name	$f_{Ca/Si}$		O	Si	Ca	Total	$EDS_{Ca/Si}$
CHMS-1	0.1	Weight %	66.89	30.38	2.73	100.00	0.09
		Atom %	78.43	20.29	1.28	100.00	
CHMS-2	0.2	Weight %	62.03	36.29	1.69	100.00	0.05
		Atom %	74.40	24.79	0.81	100.00	
CHMS-3	0.3	Weight %	67.49	25.16	7.35	100.00	0.29
		Atom %	79.63	16.91	3.46	100.00	
CHMS-5	0.5	Weight %	67.42	23.65	8.93	100.00	0.38
		Atom %	79.83	15.95	4.22	100.00	

[a] Notation: $f_{Ca/Si}$= Ca/Si molar ratio in the synthesis gel; $EDS_{Ca/Si}$ = Ca/Si ratio based on the weight% of the Ca and Si species.

clearly seen from the TEM image, which is a typical characteristic of mesoporous materials.

TEM images of the Li-doped silica samples are shown in Fig. 6(a) and (b). The image in Fig. 6(a) shows the typical mesostructured nature of the LHMS-5 sample with a highly ordered hexagonal array of pores. The lighter area indicates the shape of the mesopores, which are about 3.0–3.8 nm in size. This result from TEM is in accordance with the data obtained from SAXS and N_2 sorption.

3.6. N_2 adsorption–desorption

N_2 adsorption–desorption isotherms were recorded for Ca and Li-doped porous silicas in order to determine the BET specific surface area (S_{BET}), total pore volume (V_P), and average pore diameter (D_{KJS}) of the materials. Fig. 7(a) shows nitrogen sorption isotherms for the Ca-doped silica samples (CHMS-1,-2, -3, and -5). The respective physicochemical parameters evaluated from these isotherms are listed in Table 1. The isotherms of all CHMS samples are typical type IV isotherms according to the IUPAC classification, representing the mesoporous nature of the materials. The hysteresis loop in the isotherm at higher P/P_0 also indicates capillary condensation and desorption in open-ended cylindrical mesopores, which is characteristic of a material having cylindrical geometries with uniform pore size.[27] However, in the initial stage the N_2 volume consumed due to monolayer adsorption is very much less for CHMS-1 and CHMS-3, indicating a drastically low BET surface area (Table 1). The other two samples, CHMS-2 and CHMS-5, show a significant quantity of monolayer adsorption, indicating a very high surface area (315–318 $m^2\ g^{-1}$). Also both the samples show very broad hysteresis with capillary condensation located at values of P/P_0 of about 0.45–0.80.

The corresponding pore size distribution (PSD) plots of all CHMS samples measured by the KJS method are given in Fig. 7(b). The narrow PSD curves indicate the presence of uniform pores in the materials. The pore diameters (D_{KJS}) of

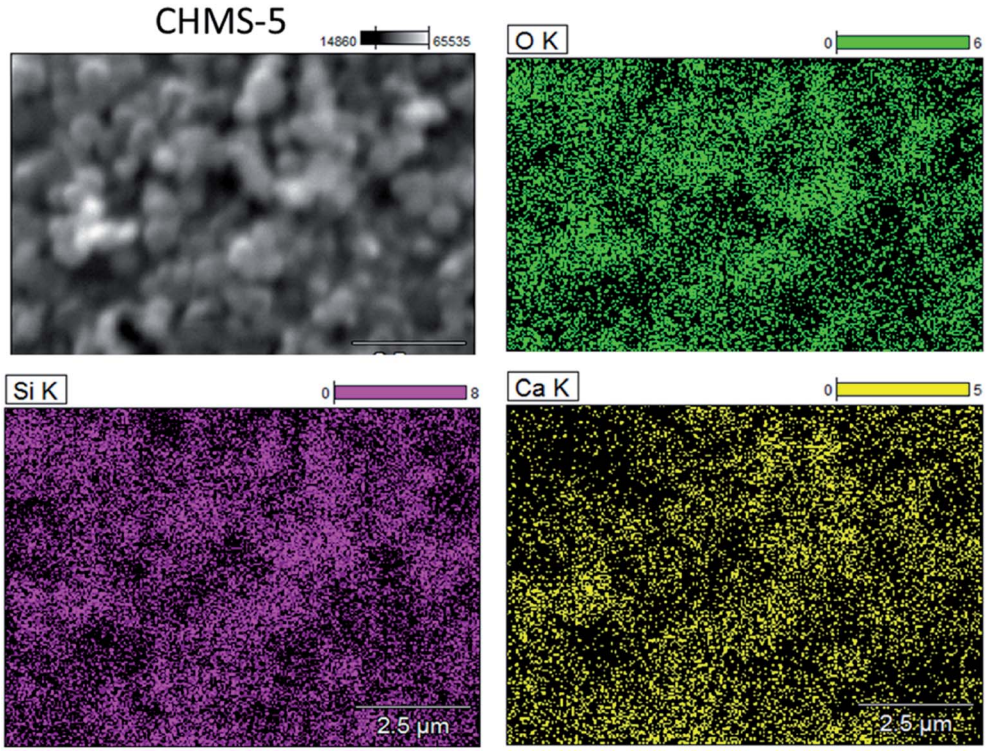

Fig. 4 SEM-EDS mapping images for CHMS-5 sample.

CHMS-2 and CHMS-5 determined at the maxima in the PSD plots are in the range from 3.2 to 3.4 nm, which is typical for a mesoporous material synthesized using a CTAB surfactant. The pore width of the CHMS-5 sample (D_{KJS}) obtained from the pore size distribution plot is 3.42 nm, which matches well with the pore size obtained from the TEM image as well as the *d*-spacing value obtained from the SAXS data. Due to the low surface area, the two samples, CHMS-1 and CHMS-3, show an abnormal PSD and very high pore diameters. The reason behind this may be that the Ca/Si molar ratios of 0.2 and 0.5 must be the most optimised compositions for the preparation of this Ca-doped silica material.

N_2 sorption isotherms for all Li-doped silica samples are displayed in Fig. 8(a). All LHMS samples show typical type IV isotherms, representing the mesoporous characteristic of the materials. For each sample a good amount of monolayer adsorption is observed, indicating appreciably high surface areas in the range 323–743 $m^2 g^{-1}$. The hysteresis loop is very narrow or almost negligible in these cases. The capillary condensation steps are observed to be at a relative pressure $P/P_0 = 0.2$–0.4 and the pore volume (V_P) is in the range 0.39–0.59 $cm^3 g^{-1}$.

The PSD plots of the LHMS-1 to −5 samples are shown in Fig. 8(b). All the samples show very narrow PSD curves, indicating the presence of uniform mesopores throughout the

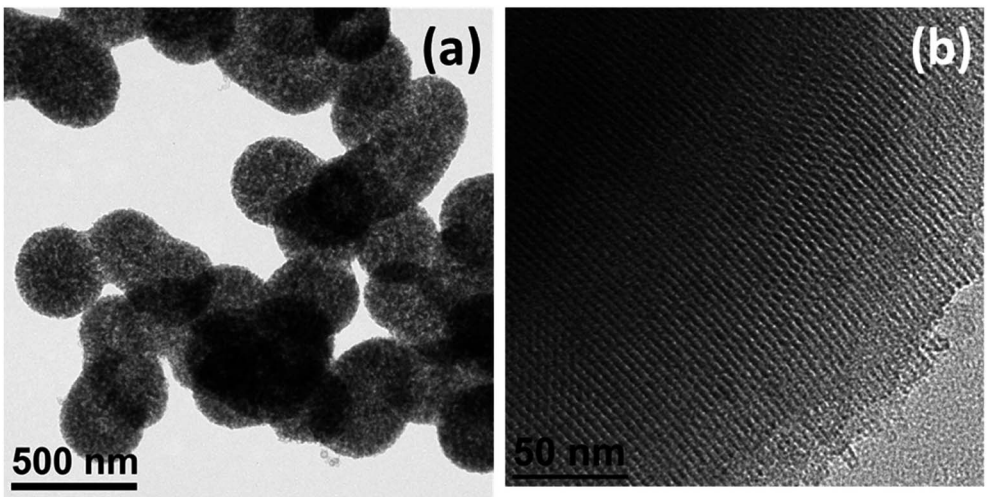

Fig. 5 (a) TEM images of the Ca-doped silica sample. (b) TEM image of the CHMS-5 at high resolution.

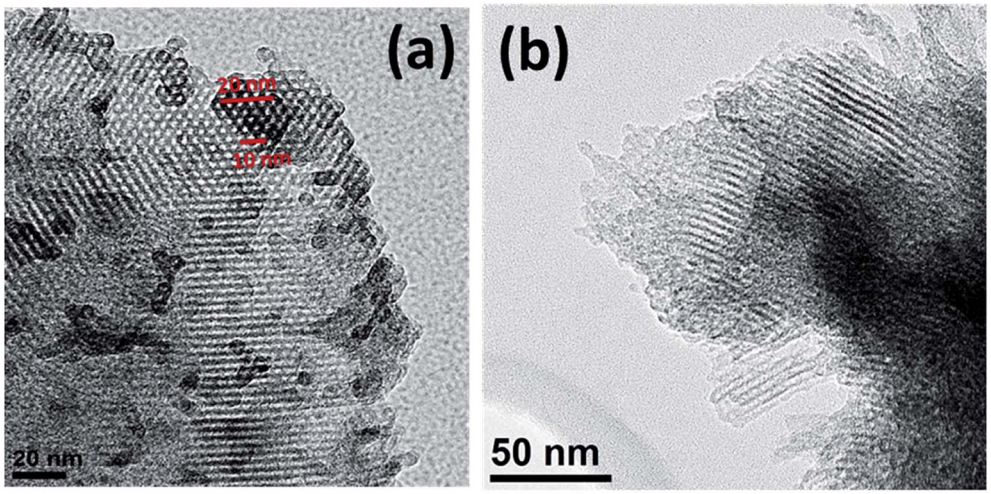

Fig. 6 (a) TEM images of the LHMS-5. (b) TEM image of the LHMS-5 viewed along (110) plane.

sample. The pore diameters (D_{KJS}) obtained from PSD maxima are in the range 3.0–3.3 nm (Table 1), which match well with the *d*-spacings as well as the pore sizes obtained from the TEM images of the Li-silica samples. With the increase in the Li content from LHMS-1 to LHMS-5, the surface area of the sample should decrease, due to a decrease in ordering in the respective mesostructure with increasing metal incorporation. However, the surface area and pore volume are significantly less for the LHMS-2 sample, indicating a lower ordering in the mesostructure.

3.7. H_2 and CO_2 gas adsorption

Due to high surface area and good pore diameter, mesoporous Ca and Li-doped silica materials have been explored for storage of both H_2 and CO_2 gas uptake under atmospheric pressure and at 25 °C temperature for about 180 min (3 h) duration. The time-dependant H_2 and CO_2 gas uptake mixed with N_2 gas over CHMS-1 and CHMS-5 samples is given in Fig. 9(a) and (b), respectively. To estimate individually the H_2 and CO_2 gas uptake from the mixed gas flow, the uptake amount of pure N_2 gas has to be found. In Fig. 9(a), it is observed from the adsorption isotherm of N_2 at 25 °C and 1 atm. that the maximum uptake for pure N_2 gas obtained is 100.6 wt% for 3 h. The uptakes for mixed gas CO_2/N_2 and H_2/N_2 are 102.3 wt% and 101.1 wt%, respectively, for the CHMS-1 sample. Similarly, the CHMS-5 sample (Fig. 9(b)) uptakes for pure N_2, CO_2/N_2 and H_2/N_2 are 100.1 wt%, 102.5 wt% and 102.0 wt%, respectively, at 25 °C and 1 atm pressure.

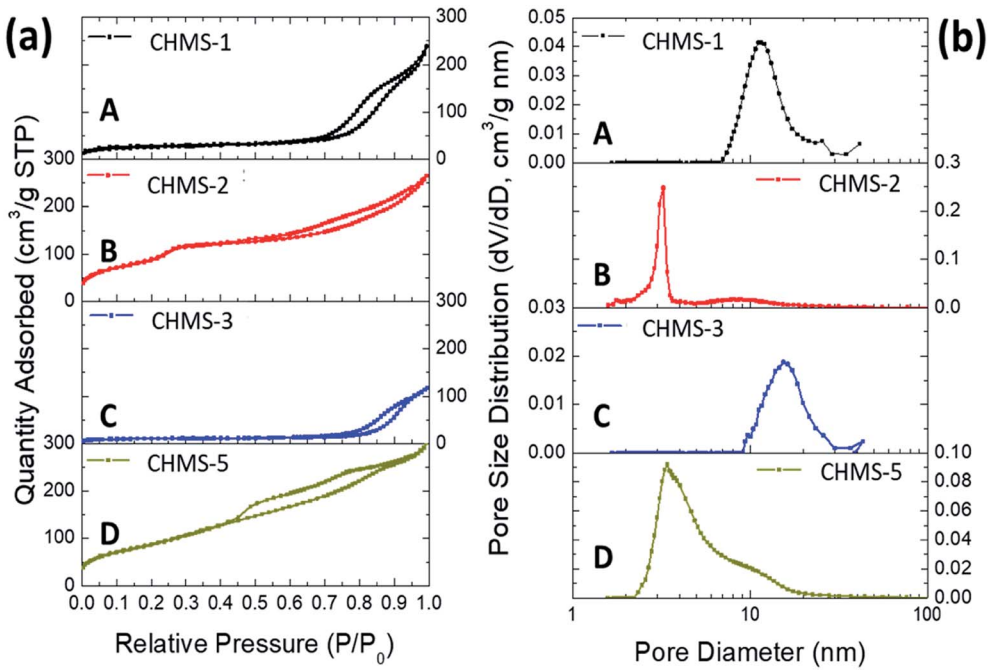

Fig. 7 (a) N_2 adsorption–desorption isotherms for (A) CHMS-1, (B) CHMS-2, (C) CHMS-3, and (D) CHMS-5 samples. (b) Corresponding pore size distribution (PSD) curves of the samples for (A) CHMS-1, (B) CHMS-2, (C) CHMS-3, and (D) CHMS-5 obtained by KJS method.

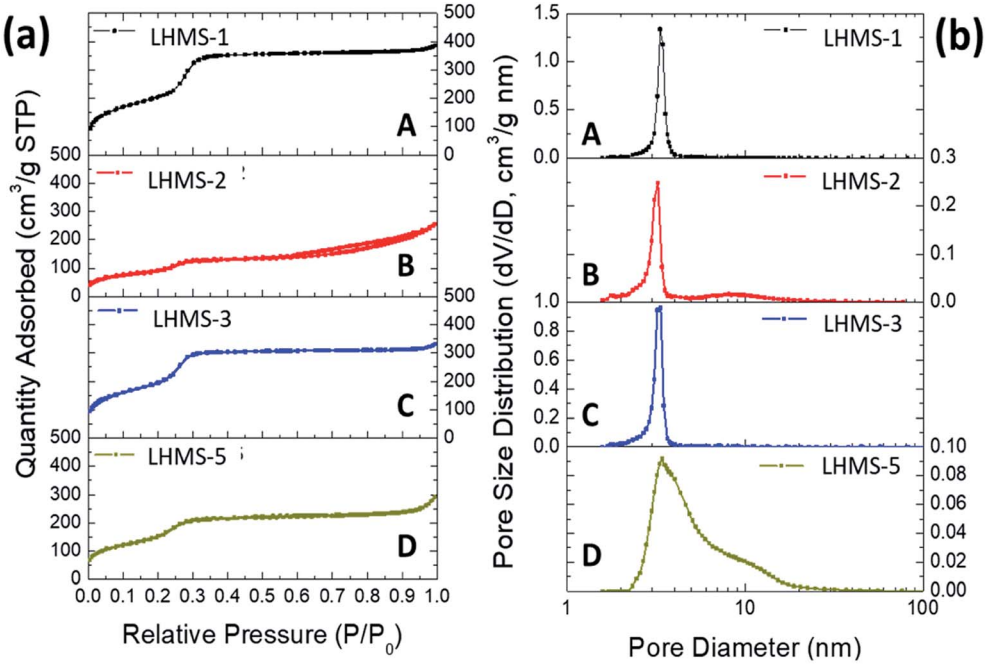

Fig. 8 (a) N_2 adsorption–desorption isotherms for (A) LHMS-1, (B) LHMS-2, (C) LHMS-3, and (D) LHMS-5 samples. (b) Corresponding pore size distribution (PSD) curves of the samples for (A) LHMS-1, (B) LHMS-2, (C) LHMS-3, and (D) LHMS-5 obtained by KJS method.

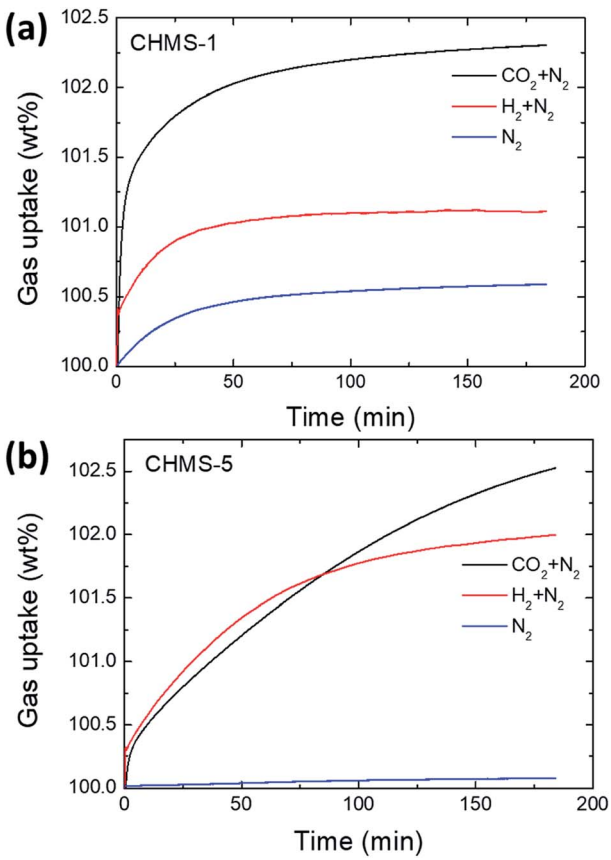

Fig. 9 Selective CO_2 and H_2 gas uptake of pure CHMS samples at 25 °C and 1 atm. Gas uptakes under mixed flows of CO_2 + N_2 gases, H_2+ N_2 gases and pure N_2 gas for (a) CHMS-1 and (b) CHMS-5 samples.

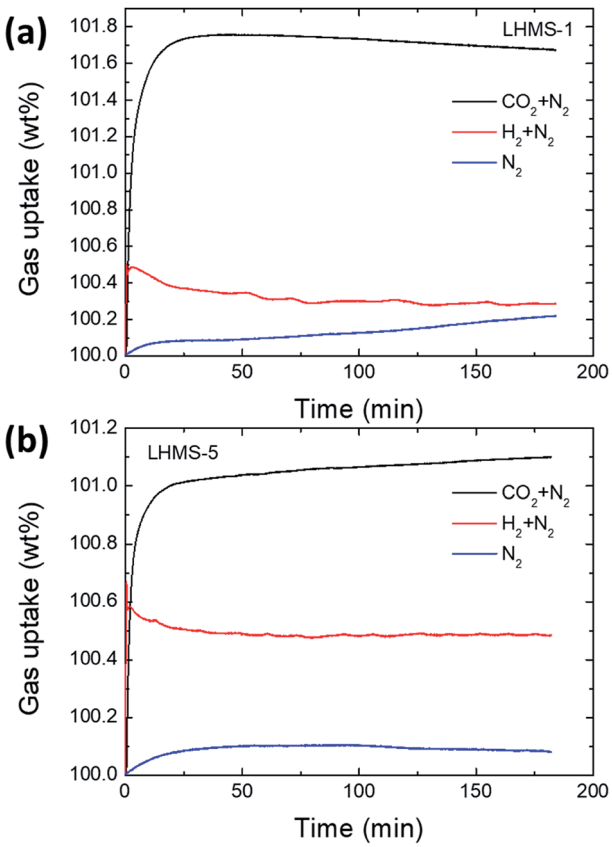

Fig. 10 Selective CO_2 and H_2 gas uptake of pure LHMS samples at 25 °C and 1 atm. Gas uptakes under mixed flows of CO_2 + N_2 gases, H_2+ N_2 gases and pure N_2 gas for (a) LHMS-1 and (b) CHMS-5 samples.

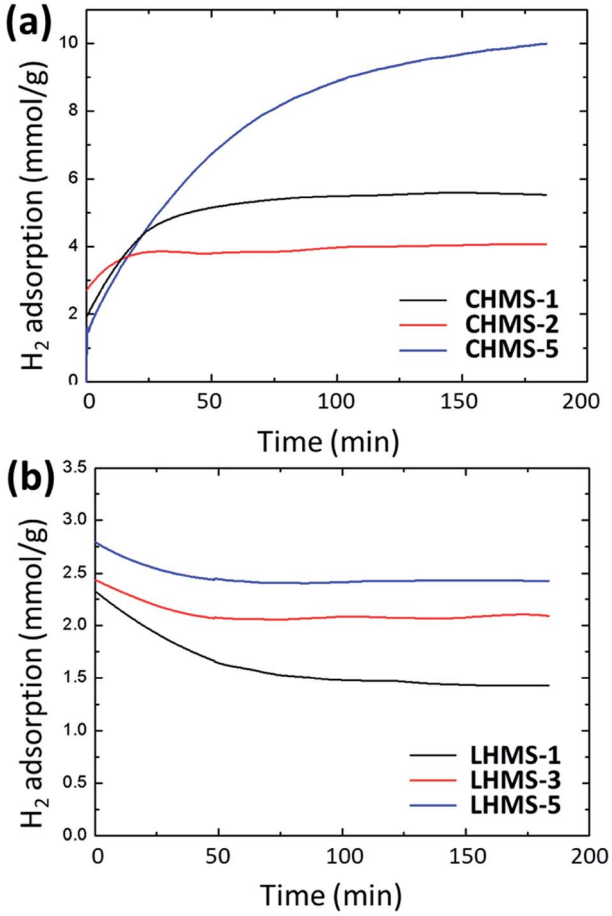

Fig. 11 Selective gas uptake of H_2 calibrated by subtracting N_2 gas uptake for (a) CHMS and (b) LHMS samples.

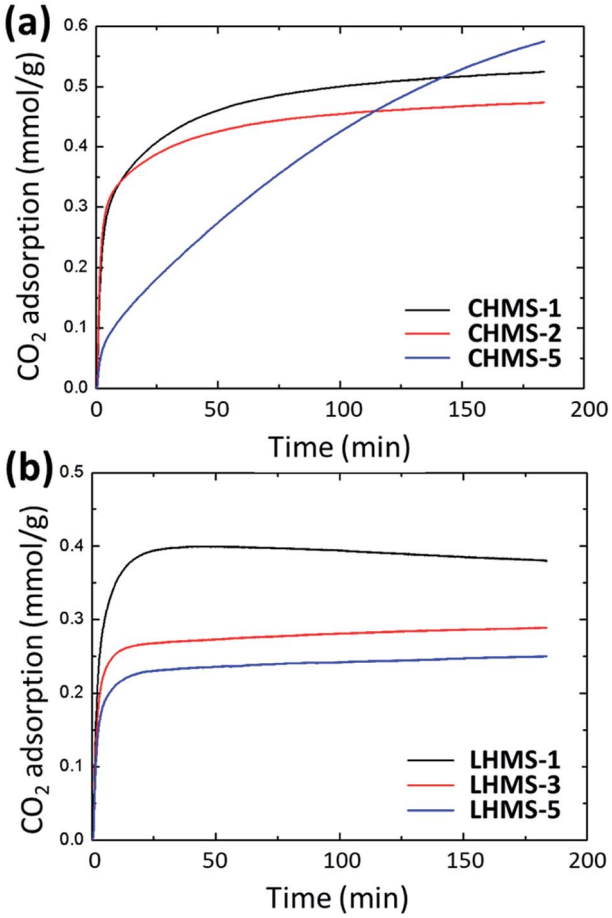

Fig. 12 Selective gas uptake of CO_2 calibrated by subtracting N_2 gas uptake for (a) CHMS and (b) LHMS samples.

In the same way as for the LHMS samples, the gas uptake measurement was carried out under the same experimental conditions (25 °C and 1 atm) and the results are shown in Fig. 10(a and b). Gas uptakes for pure N_2, CO_2/N_2 and H_2/N_2 are 100.2, 101.65, and 100.3 wt%, respectively, for the LHMS-1 sample and 100.1, 101.1, and 100.5 wt%, respectively, for the LHMS-5 sample. It can clearly be assumed from the above gas values that the N_2 amount is the maximum uptake among the mixed gases, considering competitive adsorption between two gas molecules.

Fig. 11(a and b) represents the value of H_2 gas uptake after subtracting the pure N_2 uptake appearing in Fig. 9 and 10. All the data are given in Table 4. For the CHMS-2 and -5 samples the H_2 uptake in 3 h for 1 g of Ca-doped silica sample is estimated to be 4 mmol and 10 mmol, respectively. For LHMS samples the H_2 uptake values are 1.45 (for LHMS-1), 2.1 (for LHMS-3) and 2.45 mmol g^{-1} (LHMS-5), respectively, for 3 h. The limitation of H_2 gas adsorption using Li-doped mesoporous silica can be explained by the very small amount of Li inside the pore wall.

An analogous calibration was also considered for CO_2 uptake. Fig. 12 show the values for selective CO_2 uptake for all LHMS and CHMS samples after subtracting the pure N_2 uptake from the value of the CO_2/N_2 mixed gas uptake. According to Fig. 12(a), CO_2 uptake for CHMS-2 is 0.47 mmol g^{-1} and for CHMS-5 is 0.58 mmol g^{-1} for 3 h at 25 °C and 1 atm pressure. From Fig. 12(b), it is evident that CO_2 uptake for LHMS-1, LHMS-3 and LHMS-5 are 0.38, 0.29 and 0.25 mmol g^{-1}, respectively (Table 4).

Table 4 H_2 and CO_2 uptake data over CHMS and LHMS samples

Sample	H_2 (mmol g^{-1})	CO_2 (mmol g^{-1})	CO_2 by amine-silica (mmol g^{-1})	CO_2 at 393 K (mmol g^{-1})
CHMS-1	5.50	0.52	0.67	0.13
CHMS-2	4.00	0.47	0.50	0.04
CHMS-5	10.00	0.58	0.54	0.10
LHMS-1	1.45	0.38	0.58	0.05
LHMS-3	2.10	0.29	0.35	−0.05
LHMS-5	2.45	0.25	0.34	−0.044

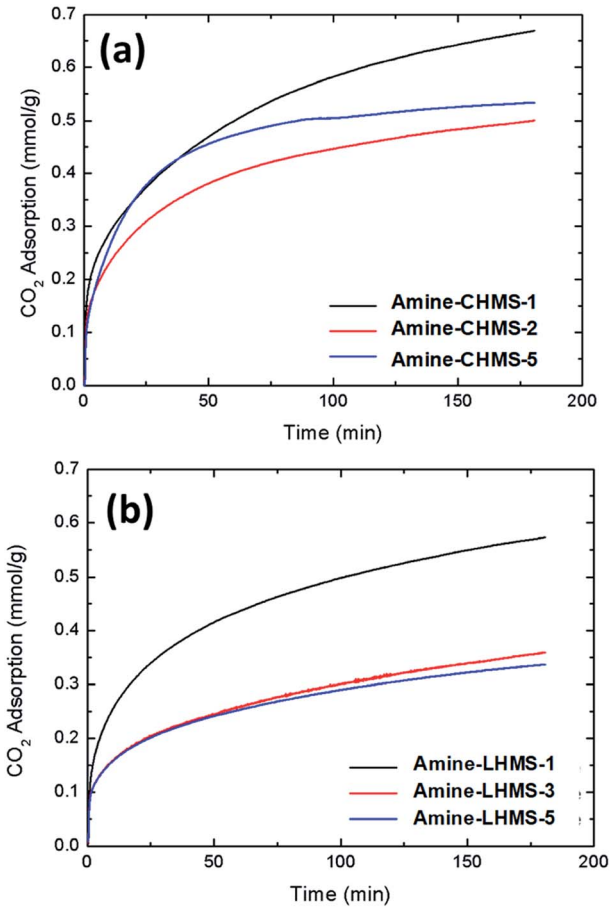

Fig. 13 Selective gas uptake of CO_2 calibrated by subtracting N_2 gas uptake for all amine-modified samples. (a) Amine-CHMS and (b) amine-LHMS samples.

Ca and Li doped silica samples are functionalized with amine group which, having a Lewis basic property, may induce the adsorption of CO_2 over these materials.[1,2] On the other hand, the surface area and pore volume as well as the CO_2 uptake amount of mesostructured materials modified with amine groups may drastically change due to the presence of the functional groups in the pore walls.[1] Fig. 13 shows the effect of amine modified CHMS and LHMS samples on CO_2 adsorption under the same experimental conditions. By subtracting the N_2 uptake value (Fig. 13(a)), CO_2 uptake for amine-CHMS-2 and amine-CHMS-5 are 0.5 mmol g^{-1} and 0.54 mmol g^{-1}, respectively (Table 4). Selective CO_2 adsorptions recorded for amine-LHMS samples (Fig. 13(b)) are 0.58 (LHMS-1), 0.35 (LHMS-3) and 0.34 mmol g^{-1} (LHMS-5), respectively. Compared to the pure metal doped silicas, amine-modified silicas show very little increase in the amount of CO_2 uptake (Table 4), which can be attributed to the improved basicity of the materials useful for CO_2 (a Lewis acid) adsorption. Although in the case of CHMS-5 the value is little lower in the case of amine modification, which may be due to partial pore blockage because of the extra loading of amine over a high percentage of metal doping.[2]

CO_2 gas uptake at an elevated temperature, say 120 °C, and normal pressure (1 atm) has also been studied to understand the effect of temperature on the adsorption quantity. Fig. S3(a and b) (in ESI†) demonstrates the effect of temperature on the CO_2 adsorption quantity of both the Ca and Li doped mesoporous silica samples. CO_2 uptake by the CHMS-1 and CHMS-5 samples at 120 °C are 0.04 mmol g^{-1} and 0.1 mmol g^{-1}, respectively. The value for LHMS-1 is 0.05 mmol g^{-1}, whereas the quantity is somewhat abnormally low for the other two Li-samples: −0.05 and −0.044, respectively, for LHMS-2 and LHMS-5. All the data for H_2 and CO_2 uptake are given here in tabular form (Table 4). From the result it is understood that with increasing temperature the adsorption quantity decreases for all Ca and Li doped samples.

From the above H_2 and CO_2 gas adsorption measurement study, it can clearly be observed that our metal doped silica (mainly Ca-doped silica) materials are quite good at CO_2 and H_2 adsorption at ambient temperature and pressure, and the adsorption capacity more or less increases with an increase in the Li and Ca content in the silica framework. High gas adsorption (especially for H_2 gas) at normal temperature can be attributed to the presence of Lewis basic metal ions in the silica mesostructures as well as the adsorption experiments carried out in mixed flow with N_2 gas, which plays a crucial role in creating a hydrophobic non-polar environment suitable for H_2 adsorption.[16] A comparison of the adsorption capacity of the Ca-doped silica (CHMS-5) sample with other adsorbents from the literature is shown in Table 5. It is clear that our material is highly economic as an adsorbent for both CO_2 and H_2 under ambient conditions compared to other reported adsorbents.

The reversibility of H_2 adsorption has been tested with the CHMS-5 sample and the results are given in Fig. S5 (ESI†). The result shows that the performance of our sample is quite satisfactory up to 9 cycles, which means that the sample can be used as an economic, stable H_2 gas adsorbent for practical purposes.

Table 5 Economic comparison of the H_2 and CO_2 uptake of CHMS and LHMS adsorbents with other samples reported in the literature

Adsorbent	Conditions	H_2 uptake (mmol g^{-1})	CO_2 uptake (mmol g^{-1})	Reference
Porous CaO	2 °C temp and 36 bar pressure	—	11.3	28
Silica gel	30 °C temp and 1 atm pressure	—	0.41	29
Hydrogen titanate nanotube	25 °C temp and 1 atm pressure	12.5	0.88	16
Zeolite template carbon	25 °C temp and 30 MPa pressure	8.3	—	30
Amine-MCM-41	30 °C temp and 0.1 bar pressure	—	0.70	2
MCM-41	30 °C temp and 0.1 bar pressure	—	0.12	2
CHMS-5	25 °C temp and 1 atm pressure	10.00	0.58	This work

4. Conclusions

In a nutshell, a one-pot soft-template CTAB mediated hydrothermal route in basic water-ethanol media has been proposed here for the syntheses of different Ca- and Li-doped hexagonally ordered mesoporous silica materials. Nitrogen sorption isotherms have shown narrow pore size distributions as well as quite high surface areas up to 315 $m^2 g^{-1}$ for a Ca-doped sample with Ca/Si = 0.5 in the synthesis gel and 543 $m^2 g^{-1}$ for an Li-doped sample with Li/Si = 0.5. However, according to ICP-AES, Li incorporation into the samples is almost negligible and a very small amount of Li content up to 0.044 wt% is observed in the sample, although the Ca contents vary from 4.5 to 15 wt% in various Ca-silica samples. The low Li content in silica can be attributed to the high ionizing tendency of Li ions, because of which some of the metal ions leach through filtration as well as during sol–gel reaction without binding with silica species. The sample Ca-doped silica CHMS-5 exhibits significant H_2 adsorption up to 10 mmol g^{-1} and CO_2 adsorption up to 0.58 mmol g^{-1} at normal temperature and pressure. Moreover, the reversibility for H_2 uptake has been fulfilled by the CHMS-5 sample. From this work it can be concluded that our Ca-doped mesoporous silica samples can be used as highly potential and practical adsorbents for energy-effective H_2 storage application.

Conflicts of interest

There are no conflicts to declare.

Acknowledgements

This study was supported by the Research Program funded by the Seoul Tech (Seoul National University of Science and Technology). Experiments at PLS-II were supported in part by MSICT and POSTECH.

References

1 K. Sim, N. Lee, J. Kim, E.-B. Cho, C. Gunathilake and M. Jaroniec, *ACS Appl. Mater. Interfaces*, 2015, **7**, 6792–6802.
2 M. R. Mello, D. Phanon, G. Q. Silveira, P. L. Llewellyn and C. M. Ronconi, *Microporous Mesoporous Mater.*, 2011, **143**, 174–179.
3 S. Clauzier, L. Ngoc Ho, M. Pera-Titus, D. Farrusseng and B. Coasne, *J. Phys. Chem. C*, 2014, **118**, 10720–10727.
4 L. Zang, S. Liu, H. Guo, X. Chang, X. Xu, L. Jiao, H. Yuan and Y. Wang, *Chem.–Asian J.*, 2018, **13**, 350–357.
5 J. hui Lan, D. Cao and W. Wang, *ACS Nano*, 2009, **3**, 3294–3300.
6 L. Fu, K. Tang, H. Oh, K. Manickam, T. Bräuniger, C. Vinod Chandran, A. Menzel, M. Hirscher, D. Samuelis and J. Maier, *Nano Lett.*, 2015, **15**, 4170–4175.
7 M. Kubo, H. Ushiyama, A. Shimojima and T. Okubo, *Adsorption*, 2011, **17**, 211–218.
8 Y. Xia, Z. Yang and Y. Zhu, *J. Mater. Chem. A*, 2013, **1**, 9365–9381.
9 G. Perot and M. Guisnet, *J. Mol. Catal.*, 1991, **61**, 173–196.
10 J. Dong, X. Wang, H. Xu, Q. Zhao and J. Li, *Int. J. Hydrogen Energy*, 2007, **32**, 4998–5004.
11 T. H. Kwon, S. Jung, H. J. Kim, S. Park, S. J. Kim and S. Huh, *Eur. J. Inorg. Chem.*, 2009, **19**, 2811–2816.
12 M. Paik Suh, H. J. Park, T. K. Prasad and D. W. Lim, *Chem. Rev.*, 2012, **112**, 782–835.
13 Y. Huang, C. Yang, Z. Sun, G. Zenga and H. He, *RSC Adv.*, 2015, **5**, 11475–11484.
14 Y. Cheng, C. Yang, H. He, G. Zeng, K. Zhao and Z. Yan, *J. Environ. Eng.*, 2016, **142**, C4015001.
15 H. J. He, Z. H. Xiang, X. J. Chen, H. Chen, H. Huang, M. Wen and C. P. Yang, *Int. J. Environ. Sci. Technol.*, 2018, **15**, 1491–1500.
16 S. Sim, E.-B. Cho and S. Chatterjee, *Chem. Eng. J.*, 2016, **303**, 64–72.
17 P. Carraro, V. Elias, A. Garcia Blanco, K. Sapag, S. Moreno, M. Oliva and G. Eimer, *Microporous Mesoporous Mater.*, 2014, **191**, 103–111.
18 S.-C. Chang, S.-Y. Chien, C.-L. Chen and C.-K. Chen, *Appl. Surf. Sci.*, 2015, **331**, 225–233.
19 S. Loganathan, M. Tikmani and A. K. Ghoshal, *Langmuir*, 2013, **29**, 3491–3499.
20 J. Baltrusaitis and V. H. Grassian, *J. Phys. Chem. B*, 2005, **109**, 12227–12230.
21 N. Florin and P. Fennell, *Energy Procedia*, 2011, **4**, 830–838.
22 N. Pal, S. Banerjee, E. Choi and E.-B. Cho, *ChemistrySelect*, 2018, **3**, 6029–6034.
23 H. Furukawa and O. M. Yaghi, *J. Am. Chem. Soc.*, 2009, **131**, 8875–8883.
24 M. Kruk, M. Jaroniec and A. Sayari, *Langmuir*, 1997, **13**, 6267–6273.
25 N. Pal, E.-B. Cho, D. Kim and M. Jaroniec, *J. Phys. Chem. C*, 2014, **118**, 15892–15901.
26 J. Tua, R. Wang, W. Genga, X. Lai, T. Zhang, N. Li, N. Yue and X. Li, *Sens. Actuators, B*, 2009, **136**, 392–398.
27 P. I. Ravikovitch and A. V. Neimark, *J. Phys. Chem. B*, 2001, **105**, 6817–6823.
28 N. Azmi, S. Yusup and K. M. Sabil, *J. Cleaner Prod.*, 2017, **168**, 973–982.
29 O. Leal, C. Bolivar, C. Ovalles and J. J. Garcia andY.Espidel, *Inorg. Chim. Acta*, 1995, **240**, 183–189.
30 N. P. Stadie, J. J. Vajo, R. W. Cumberland, A. A. Wilson, C. C. Ahn and B. Fultz, *Langmuir*, 2012, **28**, 10057–10063.